Eur. Phys. J. B **66**, 37–40 (2008)
DOI: 10.1140/epjb/e2008-00385-4

THE EUROPEAN PHYSICAL JOURNAL B

Angular dependence of the transverse and vortex modes in magnetic nanotubes

S. Allende[1,a], J. Escrig[1], D. Altbir[1], E. Salcedo[2], and M. Bahiana[3]

[1] Departamento de Física, Universidad de Santiago de Chile, USACH, Av. Ecuador 3493, Santiago, Chile
[2] Instituto de Física, Universidade Federal do Rio Grande do Sul, CP 15051, 91501-970 Porto Alegre, RS, Brazil
[3] Universidade Federal do Rio de Janeiro, Instituto de Física, CP 68528, 21941-972 Rio de Janeiro, Brazil

Received 29 April 2008 / Received in final form 11 August 2008
Published online 11 October 2008 –

Abstract. The angular dependence of the transverse and vortex modes in a magnetic nanotube is investigated as a function of the tube geometry, by means of analytical calculations and numerical simulations. A critical radius defining the transition between vortex and transverse reversal modes is determined, leading to low or high coercivity modes just by varying the direction of the external field, in a fixed nanotube.

PACS. 73.63.Fg Nanotubes – 74.25.Ha Magnetic properties

1 Introduction

As fabrication technology pushes the dimensions of structures into the nanoscale, understanding the magnetization processes of these nanostructures becomes an important issue for its applications in spintronic devices [1,2]. For most of these applications, spherical and cylindrical particles have been the preferred. However, since these shapes have only one surface for modification, the generation of multifunctional objects turns out to be limited. Since 2004 magnetic nanotubes have been grown providing particles with two adjustable surfaces (internal and external) [3–5]. Nanotubes have magnetic properties that allow them to be traced directly using magnetic resonance imaging, making them useful in diagnosis applications [6]. Also, they are interesting for different biological applications [4] since they are able to float in solutions due to their low density.

One of the most important properties of nanomagnets is the coercivity, which is strongly dependent on geometric parameters. Although the current experimental facilities allow the fabrication of tubes with a variety of geometries, precision is still a problem. A given fabrication procedure may yield tubes with wall thickness with a typical dispersion of 3 nm in thin nanotubes [7]. Therefore, the possibility of controlling the coercivity by other means is highly desirable. Since coercivity is directly related to the reversal mechanism, one alternative is to induce different reversal modes by modifying external parameters, such as the direction of the applied field.

In this work we investigate, using an analytical model and numerical simulations, the angular dependence of the magnetization reversal of Ni nanotubes, considering the different modes that can be present, as a function of the tubes geometry. We focus on small diameter nanotubes such as the ones reported by Bachmann et al. [8] and Daub et al. [9].

2 Models

Geometrically, tubes are characterized by their external and internal radii, R and a, respectively, and length L. It is convenient to define the ratio $\beta \equiv a/R$, so that $\beta = 0$ represents a solid cylinder and β close to 1 corresponds to a very narrow tube. Besides, we consider an external magnetic field H_a applied in a direction defined by θ, which is the angle between the applied field direction and the tube axis, as illustrated in Figure 1a.

2.1 Numerical model

The different reversal modes were found via Monte Carlo simulations. In this case the energy E of a nanotube with N magnetic moments was written as $E = \sum_{j>i}^{N} E_{ij}^{d} - J\sum_{ij\in\{nn\}} \hat{\mu}_i \cdot \hat{\mu}_j + E_a$, where E_{ij}^{d} is the dipolar energy given by $E_{ij}^{d} = \left[\boldsymbol{\mu}_i \cdot \boldsymbol{\mu}_j - 3(\boldsymbol{\mu}_i \cdot \hat{n}_{ij})(\boldsymbol{\mu}_j \cdot \hat{n}_{ij})\right]/r_{ij}^{3}$, with r_{ij} being the distance between the magnetic moments $\boldsymbol{\mu}_i$ and $\boldsymbol{\mu}_j$, $\hat{\mu}_i$ the unit vector along the direction of $\boldsymbol{\mu}_i$, and $\hat{n}_{ij}$, the unit vector along the direction that connects $\boldsymbol{\mu}_i$ and $\boldsymbol{\mu}_j$. J is the exchange coupling constant between nearest neighbors and $E_a = -\sum_{i=1}^{N} \boldsymbol{\mu}_i \cdot \boldsymbol{H}_a$. Our nickel nanotube was built along the [100] direction of a fcc lattice with parameter $a_0 = 3.52$ Å. We also used the values $\mu_i = 0.61\ \mu_B$ and $J = 3.5$ meV. We have investigated tubes with R varying between 10 and 25 nm, and

[a] e-mail: sallende@fisica.usach.cl

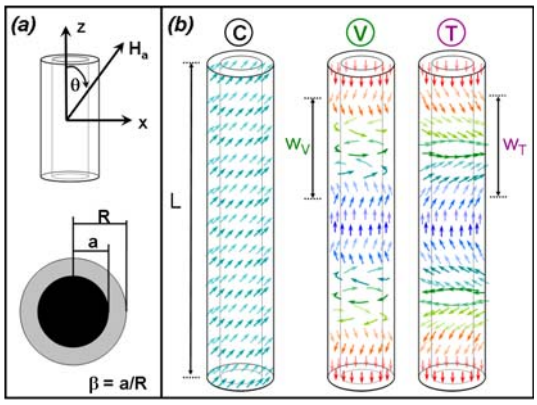

Fig. 1. (a) Geometrical parameters of a nanotube. (b) Magnetization reversal modes in nanotubes. The arrows represent the orientation of magnetic moments within the tube. Left: coherent-mode rotation, C. Center: vortex-mode rotation, V, with a domain wall of thickness w_V. Right: transverse-mode rotation, T, with a domain wall of thickness w_T.

$L = 0.5$ μm. Such tube contains about 10^8 atoms, which is out of reach for a regular MC simulation with dipolar interactions, considering the available computational resources. In order to reduce the number of interacting atoms we made use of a scaling technique, proposed by d'Albuquerque et al. [10], originally formulated to investigate the equilibrium phase diagram of cylindrical particles of height h and diameter d. The authors showed that this diagram is equivalent to the one for a smaller particle with $d' = d\chi^\eta$ and $h' = h\chi^\eta$, with $\chi < 1$ and $\eta \approx 0.56$, if the exchange constant is also scaled as $J' = \chi J$. We use this idea starting from the desired value for the total number of interacting particles we can deal with, based on the computational facilities currently available, and have estimated N of the order of 10^3. With this in mind we have obtained the scale value $\chi = 4 \times 10^{-3}$, leading 6048 atoms for a tube with external ratio of 25 nm and $\beta \equiv 14/30$. It has also been shown that the scaling relations can be used together with MC simulations showing good agreement with experiments and micromagnetic calculations [11–14].

MC simulations were carried out at $T = 300$ K, using the Metropolis algorithm [15] in which the new orientation of the magnetic moments is restricted according to Nowak et al. [16]. It is important to mention that Monte Carlo simulations consider essentially the energy of the system. Effects related to the magnetization dynamics, like torques and magnetization precession are not considered. In the initial state of our system $H_a = 6$ kOe, which is higher than the saturation field, and all magnetic moments were parallel to $\boldsymbol{H}_a$. The field was then linearly decreased at a rate of $\Delta H = 0.01$ kOe for every 300 MC steps. In this way, about 200 000 MC steps are needed to go from saturation to the coercive field. The variation of β and θ and previous data on tubes [7,14] show three main idealized types of magnetization reversal, which are illustrated in Figure 1b. In a *coherent rotation*, C, all the spins (local magnetic moments) rotate simultaneously; in a *vortex reversal mode*, V, spins inside a wall rotate remaining tangent to the tube wall; and in the *transverse reversal mode*, T, a net magnetization component in the (x, y) plane appears inside the domain walls. In our MC simulations we observed that when $\theta = 0$ the direction of the magnetization component in the (x, y) plane of the transverse domain wall rotates during reversal. Hertel and Kirschner [17] called this reversal mechanism the corkscrew mode. On the other hand, for $\theta \neq 0$, we observe that the wall magnetization lies on a plane defined by the external magnetic field and the tube axis. In this case, and considering that no precession has been included in our model, the (x, y) field components act as a unidirectional anisotropy defining a reversion plane

2.2 Analytical model

In order to obtain general information about the angular dependence of the reversal modes, we have developed analytical calculations that lead us to obtain the coercive field H_c^k assuming each of the previously mentioned reversal mechanisms, $k =$ C, T, and V. The angular dependence of the nucleation for a coherent magnetization reversal was calculated by Stoner-Wohlfarth [18] and gives

$$\frac{H_n^C}{M_0} = -\frac{1 - 3N_z(L)}{2}\frac{\sqrt{1 - t^2 + t^4}}{1 + t^2},$$

where $t = \tan^{\frac{1}{3}}(\theta)$ and M_0 is the saturation magnetization. The demagnetizing factor of a tube along the z axis has been previously obtained by Escrig et al. [19] and is given by

$$N_z(l) = \frac{2R}{l(1-\beta^2)}\int_0^\infty \frac{dy}{y^2}\left(J_1(y) - \beta J_1(\beta y)\right)^2\left(1 - e^{-y\frac{l}{R}}\right).$$

For the T mode, the angular dependence of the coercivity can be studied by an adapted Stoner-Wohlfarth model [7] in which the width of the domain wall, w_T, is used as the length of the region undergoing coherent rotation. Starting from the equations presented by Landeros et al. [14] we can calculate the width of the domain wall (Fig. 2) for the transverse mode as a function of the tube geometry. We observed wall widths between 40 and 100 nm as a function of β. Following this approach,

$$\frac{H_n^T}{M_0} = -\frac{1 - 3N_z(w_T)}{2}\frac{\sqrt{1 - t^2 + t^4}}{1 + t^2}.$$

As shown in the Stoner-Wohlfarth model [18], the nucleation field does not represent the coercivity in all cases. However, from their discussion on p. 21 [18], the coercivity for a coherent and transverse reversal can be written as

$$H_c^{C(T)} = \begin{cases} \left|H_n^{C(T)}\right| & 0 \le \theta \le \pi/4 \\ 2\left|H_n^{C(T)}(\theta = \pi/4)\right| - \left|H_n^{C(T)}\right| & \pi/4 \le \theta \le \pi/2. \end{cases}$$

In very short tubes ($L \approx w_T$) the energy cost involved in the creation of a domain wall gives rise to a coherent mode of reversal.

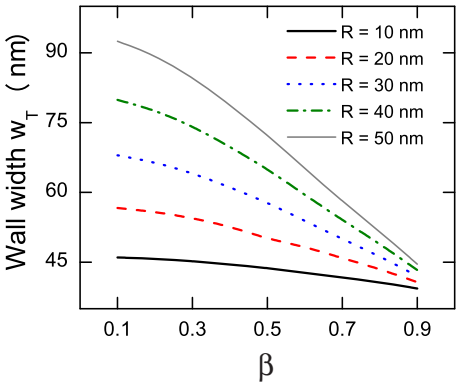

Fig. 2. Domain wall width as a function of β for the T mode of magnetization reversal.

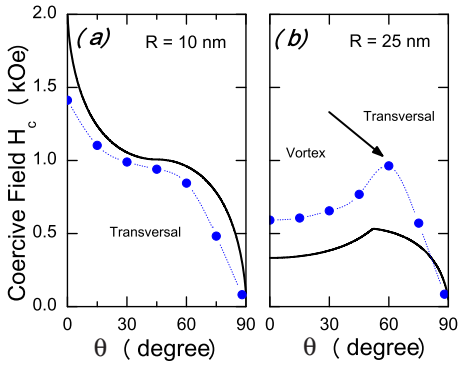

Fig. 3. Angular dependence of the coercivity, H_c, in a Ni nanotube with $L = 0.5$ μm, $\beta = 14/30$, and *(a)* $R = 10$ nm, and *(b)* $R = 25$ nm.

The angular dependence of the curling nucleation field in a finite prolate spheroid was obtained by Aharoni [20]. Recently, Escrig et al. [7] extended the expression for the switching field to take into account the internal radii of tubes, obtaining

$$\frac{H_n^V}{M_0} = \frac{\left(N_z - \frac{q^2 L_x^2}{R^2}\right)\left(N_x - \frac{q^2 L_x^2}{R^2}\right)}{\sqrt{\left(N_z - \frac{q^2 L_x^2}{R^2}\right)^2 \sin^2\theta_0 + \left(N_x - \frac{q^2 L_x^2}{R^2}\right)^2 \cos^2\theta_0}},$$

with q satisfying [21]

$$\frac{qJ_0(q) - J_1(q)}{qY_0(q) - Y_1(q)} - \frac{\beta q J_0(\beta q) - J_1(\beta q)}{\beta q Y_0(\beta q) - Y_1(\beta q)} = 0. \qquad (1)$$

Here $J_p(z)$ and $Y_p(z)$ are Bessel functions of the first and second kind, respectively. Equation (1) has an infinite number of solutions, of which only the one with the smallest nucleation field has to be considered [22]. As pointed out by Aharoni [20], for a prolate spheroid with $\theta_0 = 0$, a jump of the magnetization at or near the curling nucleation field occurs. Therefore, the coercivity is quite close to the absolute value of the nucleation field. Then, we assumed here that $-H_n^V$ is a good approximation to the coercivity, H_c^V, when the reversal occurs in the V mode, as in other studies [7,20,23].

3 Results and discussion

With the above expressions for the coercivity it is possible to study how the geometry influences the reversal process, for different values of θ. In our model the system will reverse its magnetization by whichever mode opens an energetically accessible route first, that is, by the mode that exhibits the lowest coercivity. However, for highly dynamic cases, the path of lowest coercivity might not be accessible due to precession effects. By evaluating the coercivity of the different modes we found the one which drives the reversal for each θ. Figure 3 illustrates our results for a Ni nanotube with $L = 0.5$ μm, $\beta = 14/30$, and (a) $R = 10$ nm and (b) $R = 25$ nm. Blue dots and solid lines represent the coercivity obtained by means of numerical simulations and analytical calculations, respectively. As depicted in Figure 3a, in a small diameter tube the T mode will always be preferred. If the tube diameter is increased, Figure 3b, we can observe a transition from a V to a T mode as a function of θ. Analytically the transition between T and V modes is abrupt, since the slope of the $H_c(\theta)$ curves at the crossing point is different. Numerical simulations show a smooth transition. Around the crossing point, $\theta = 60°$, the reversal process starts at the tips of the tube with a V mode rotation, propagates, and finishes in the center of the tube with a T mode rotation.

From our analytical calculations, for both radii the coercivity is always larger in the C mode than in the T mode. However, in the limit of large angles, the values of coercivity for both modes are very close. This is in good agreement with our numerical simulations for $\theta = 88°$, where we observed a coherent rotation.

We now investigate the dependence of the reversal modes on $\beta = a/R$ and θ. Figure 4 illustrates trajectories of the critical radius, $R_c(\beta, \theta)$, at which both coercivities, from T and V modes, are equal. For $R < R_c(\beta, \theta)$ the magnetization reverses by means of transversal walls, while for $R > R_c(\beta, \theta)$ vortex walls appear. In the considered range of parameters, we found that an increase of the ratio β results in a decrease of the critical radius, enhancing the region of stability of the V reversal mode. This until $\theta = 88°$, where R_c increases with β, favoring the T reversal mode. The critical radius for $\theta = 0$, was previously obtained by Landeros et al. [14] by calculating the energy barriers for different modes. In spite of the different methodology, our results are in good agreement with those. Figure 4 can also be interpreted as a phase diagram in which each line separates the T mode of magnetization reversal, which prevails in the lower region of the (β, R) space, from the V mode, present in the upper area. Labelled dots (1) and (2) in Figure 4 correspond to the cases shown in Figure 3 with (1) $R = 10$ nm, and (2) $R = 25$ nm. In the first case, (1), the tube is in the T phase, regardless of θ, and (2) presents a V reversal mode for angles $\theta < 60°$ and a T mode for $\theta > 60°$. These quantitative results are in good agreement with our numerical simulations.

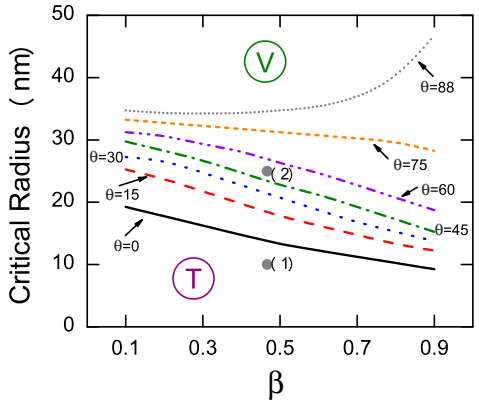

Fig. 4. Critical radius as a function of β for different angles. Points 1 and 2 are discussed in the text.

4 Conclusion

In conclusion, by means of analytical calculations and numerical simulations we have investigated the angular dependence of the reversal modes in a magnetic nanotube as a function of its geometry. We have derived analytical expressions that allow us to obtain the angular dependence of the coercivity for different reversal modes that can exist in a nanotube, leading to a critical radius defining the transition between vortex and transverse reversal modes. As a consequence, we have shown that it is possible to obtain low or high coercivity modes just by varying the direction of the external field, in a fixed nanotube, The transverse mode is present in tubes with $R < R_c(\beta, \theta)$ while for tubes with $R > R_c(\beta, \theta)$ it is always the vortex mode that controls the magnetization reversal. We also found in our Monte Carlo simulations that for $\theta = 0$, a rotation of the transversal wall along the tube axis is superimposed to the propagation, while for $\theta \neq 0$ the magnetization of the wall lies on a fixed plane defined by the external magnetic field and the tube axis. In this last case, the (x, y) field components act as a unidirectional anisotropy, defining a plane of reversion. However, as mentioned before, our model does not include the magnetization precession. In this way, real systems may not present this fixed plane. Good agreement between numerical and analytical calculations is obtained.

This work has been partially supported by Fondecyt under proyects 11070010 and 1080300, and by Millenium Science Nucleus "Basic and Applied Magnetism" P06-022F in Chile. In Brazil we acknowledge the support from Instituto de Nanotecnologia/MCT, CNPq, FAPERJ and PROSUL/CNPq program. S.A. acknowledges the support of Conicyt for a Ph.D. fellowship, and Mecesup USA0108.

References

1. S. Sun, C.B. Murray, D. Weller, L. Folks, A. Moser, Science **287**, 1989 (2000)
2. Th. Gerrits, H.A.M. van den Berg, J. Hohlfeld, L. Bar, Th. Rasing, Nature **418**, 509 (2002)
3. Y.C. Sui, R. Skomski, K.D. Sorge, D.J. Sellmyer, J. Appl. Phys. **95**, 7151 (2004)
4. K. Nielsch, F.J. Castano, C.A. Ross, R. Krishnan, J. Appl. Phys. **98**, 034318 (2005)
5. K. Nielsch, F.J. Castano, S. Matthias, W. Lee, C.A. Ross, Adv. Eng. Mater. **7**, 217 (2005)
6. D.F. Emerich, C.G. Thanos, Expert Opin. Biol. Ther. **3**, 655 (2003)
7. J. Escrig, M. Daub, P. Landeros, K. Nielsch, D. Altbir, Nanotechnology **18**, 445706 (2007); J. Escrig, J. Bachmann, J. Jing, M. Daub, D. Altbir, K. Nielsch, Phys. Rev. B **77**, 214421 (2008)
8. J. Bachmann, J. Jing, M. Knez, S. Barth, H. Shen, S. Mathur, U. Gösele, K. Nielsch, J. Am. Chem. Soc. **129**, 9554 (2007)
9. M. Daub, M. Knez, U. Goesele, K. Nielsch, J. Appl. Phys. **101**, 09J111 (2007)
10. J. d'Albuquerque e Castro, D. Altbir, J.C. Retamal, P. Vargas, Phys. Rev. Lett. **88**, 237202 (2002)
11. P. Vargas, D. Altbir, J. d'Albuquerque e Castro, Phys. Rev. B **73**, 092417 (2006)
12. M. Bahiana, F.S. Amaral, S. Allende, D. Altbir, Phys. Rev. B **74**, 174412 (2006)
13. J. Mejia-Lopez, D. Altbir, A.H. Romero, X. Battle, Igor V. Roshchin, Chang-Peng Li, Ivan K. Schuller, J. Appl. Phys. **100**, 104319 (2006)
14. P. Landeros, S. Allende, J. Escrig, E. Salcedo, D. Altbir, E.E. Vogel, Appl. Phys. Lett. **90**, 102501 (2007)
15. K. Binder, D.W. Heermann, *Monte Carlo Simulation in Statistical Physics* (Springer, New York, 2002)
16. U. Nowak, R.W. Chantrell, E.C. Kennedy, Phys. Rev. Lett. **84**, 163 (2000)
17. R. Hertel, J. Kirschner, Physica B **343**, 206 (2004)
18. E.C. Stoner, E.P. Wohlfarth, Phil. Trans. R. Soc. A **240**, 599 (1948), reprinted in IEEE Trans. Magn. **27**, 3475 (1991)
19. J. Escrig, P. Landeros, D. Altbir, E.E. Vogel, P. Vargas, J. Magn. Magn. Mater. **308**, 233 (2007)
20. A. Aharoni, J. Appl. Phys. **82**, 1281 (1997)
21. C.-R. Chang, C.M. Lee, J.-S. Yang, Phys. Rev. B **50**, 6461 (1994)
22. A. Aharoni, *Introduction to the Theory of Ferromagnetism* (Clarendon, Oxford, 1996)
23. Y. Ishii, J. Appl. Phys. **70**, 3765 (1991)